NONLINEAR FOUR-WAVE MIXING AND SUPERCONTINUUM GENERATION IN PHOTONIC CRYSTAL FIBERS: PHASE-MATCHING ANALYSIS AND SPECTRAL CHARACTERISTICS

Dr. Rahul Kumar
PG Department of Physics,
Ram Jaipal College, Jai Prakash University, Chapra, Saran, Bihar 841301, India
Email: rahulnishu03@gmail.com

ABSTRACT

The nonlinear four-wave mixing (FWM) process and supercontinuum generation (SCG) in index-guiding silica photonic crystal fibers (PCFs) were theoretically investigated through a numerical solution of the generalized nonlinear Schrödinger equation using the split-step Fourier method. The dispersion characteristics of the PCF were engineered by varying the air-hole diameter-to-pitch ratio d/Λ from 0.4 to 0.6, yielding a zero-dispersion wavelength (ZDWs) tunable between 750 and 1050 nm. The FWM phase-matching condition, incorporating both linear dispersion and nonlinear phase contributions, was analyzed for degenerate and non-degenerate pump configurations. Numerical simulations demonstrate that for a PCF with $\Lambda = 2.3$ μm and $d/\Lambda = 0.5$, pumping at the ZDW ($\lambda_{\mathrm{ZDW}} = 880$ nm) with peak power $P_0 = 1$ W produces FWM conversion efficiencies exceeding -15 dB over a 40 nm bandwidth at an optimized fiber length of 100 m. The parametric gain bandwidth is scaled as $\Omega_{\max} \propto \sqrt{\gamma P_0/|\beta_4|}$, where γ is the nonlinear coefficient, β_4 is the fourth-order dispersion, and $\Omega_{\max}$ is the maximum frequency detuning. Supercontinuum generation was simulated for femtosecond pulses ($\tau_0 = 50$ fs, $P_0 = 10$ kW) at 800 nm in a 1 m PCF, producing a broadband spectrum spanning 450–2100 nm through the combined effects of self-phase modulation, soliton fission, dispersive wave generation, and stimulated Raman scattering. The spectral flatness and coherence properties were characterized as functions of the pump power, fiber length, and dispersion profile. The results provide design guidelines for PCF-based parametric amplifiers, wavelength converters, and broadband light sources for optical fiber communication and spectroscopic applications.

Keywords: *four-wave mixing, photonic crystal fiber, supercontinuum generation, phase matching, nonlinear fiber optics*

1. INTRODUCTION

Photonic crystal fibers (PCFs), also known as microstructured optical fibers, have revolutionized nonlinear fiber optics by offering unprecedented control over the dispersion characteristics and nonlinear response through the design of the air-hole microstructure in cladding [1, 2]. Unlike conventional optical fibers, where the dispersion is primarily determined by the material properties and core diameter, PCFs allow the zero-dispersion wavelength to be shifted across a wide spectral range by adjusting the geometrical parameters, that is, the air-hole diameter d and pitch Λ (hole-to-hole spacing) [3]. This flexibility enables efficient **nonlinear interactions** at wavelengths and power levels that are inaccessible to standard fibers.

Four-wave mixing (FWM) is a third-order nonlinear parametric process arising from the intensity-dependent refractive index (optical Kerr effect) of silica fibers [4, 5]. In the degenerate FWM process, two photons from a pump wave at frequency ω_p are annihilated to

create a signal photon at ω_s and an idler photon at ω_i, satisfying the energy-conservation condition [4]:

$$2\omega_p = \omega_s + \omega_i \qquad (1)$$

The efficiency of the FWM process is governed by the **phase-matching condition**, which requires that the linear phase mismatch be compensated for by the nonlinear phase shift. The total phase mismatch for the degenerate FWM is given by [5]:

$$\kappa = \Delta\beta + 2\gamma P_0 \qquad (2)$$

where $\Delta\beta$ is the linear propagation constant mismatch, γP_0 is the nonlinear phase shift, with γ is the nonlinear coefficient, and P_0 is pump power. The linear phase mismatch can be expanded in Taylor series around the pump frequency as follows [4, 6]:

$$\Delta\beta = \beta_2\,\Omega^2 + \frac{\beta_4}{12}\,\Omega^4 + \cdots \qquad (3)$$

where $\Omega = \omega_s - \omega_p$ is the frequency detuning and β_n denotes the n-th order dispersion coefficient evaluated at the pump wavelength.

Supercontinuum generation (SCG) represents the dramatic spectral broadening of a narrow-band input pulse propagating through a nonlinear medium [7, 8]. In PCFs, SCG can span more than two octaves when pumped near the ZDW with femtosecond pulses, driven by a cascade of nonlinear processes, including self-phase modulation (SPM), soliton fission, dispersive wave (DW) generation, and stimulated Raman scattering (SRS) [9, 10]. Pulse propagation in a PCF is governed by the **generalized nonlinear Schrödinger equation** (GNLSE) [4]:

$$\frac{\partial A}{\partial z} + \frac{\alpha}{2}A - \sum_{k\geq 2}\frac{i^{k+1}\beta_k}{k!}\frac{\partial^k A}{\partial T^k} = i\gamma\left(1 + \frac{i}{\omega_0}\frac{\partial}{\partial T}\right)\left(A\int_{-\infty}^{\infty} R(T')|A(z,T-T')|^2\,dT'\right) \qquad (4)$$

where $A(z,T)$ is the slowly varying pulse envelope, α is the fiber loss, β_k is the dispersion coefficient, ω_0 is the carrier frequency, and $R(T)$ is the Raman response function.

The nonlinear response function incorporates both instantaneous Kerr and delayed Raman contributions [4]:

$$R(T) = (1 - f_R)\,\delta(T) + f_R\,h_R(T) \qquad (5)$$

where $f_R = 0.18$ is the fractional Raman contribution, and $h_R(T)$ is the Raman response function for silica. The **nonlinear coefficient** γ of a PCF is given by [2, 3]:

$$\gamma = \frac{n_2\,\omega_0}{c\,A_{\text{eff}}} \qquad (6)$$

where $n_2 = 2.6 \times 10^{-20}$ m^2/W is the nonlinear refractive index of silica, c is the speed of light, and A_{eff} is the effective mode area. PCFs with small core diameters can achieve A_{eff} values as small as 1–5 μm^2, yielding nonlinear coefficients $\gamma \approx$ 30–100 W^{-1}km^{-1}, which are 10–100 times larger than those of standard single-mode fibers [2].

The objectives of this study are: (i) to analyze the dispersion engineering of index-guiding PCFs by varying the geometrical parameters d and Λ; (ii) to investigate the FWM phase-

matching conditions and conversion efficiency in PCFs for parametric amplification; (iii) to numerically simulate supercontinuum generation and characterize the spectral broadening dynamics; and (iv) to provide design guidelines for PCF-based nonlinear photonic devices for optical fiber communication and spectroscopic applications [11, 12].

2. Theoretical Framework and Numerical Methods

2.1 Dispersion Engineering of Photonic Crystal Fibers

Figure 1 illustrates the cross-sectional geometry of the index-guiding PCF considered in this study.

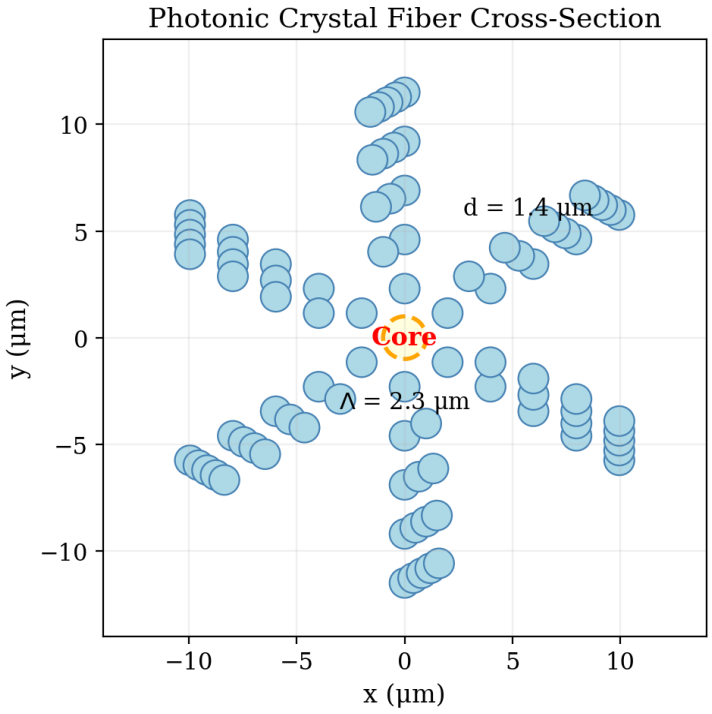

Figure 1: *Cross-sectional geometry of the index-guiding photonic crystal fiber with hexagonal lattice of air holes. The solid silica core is formed by a missing hole at the center, surrounded by five rings of air holes with pitch* $\Lambda = 2.3$ *µm and hole diameter* $d = 1.4$ *µm* $(d/\Lambda = 0.61)$.

The effective refractive index n_{eff} of the fundamental guided mode was computed using a fully vectorial finite element method (FEM) with perfectly matched layer (PML) boundary conditions [13]. The group velocity dispersion parameter β_2 was then obtained from the wavelength dependence of n_{eff} as [4]

$$\beta_2(\omega) = \frac{1}{c}\left(2\frac{dn_{\text{eff}}}{d\omega} + \omega\frac{d^2 n_{\text{eff}}}{d\omega^2}\right) \qquad (7)$$

The dispersion parameter D in conventional units is related to β_2 by $D = -2\pi c\,\beta_2/\lambda^2$. Higher-order dispersion coefficients β_3, β_4, etc., were obtained from polynomial fitting of the propagation constant $\beta(\omega)$ expanded around the pump frequency.

2.2 Phase-Matching Analysis for Four-Wave Mixing

For the degenerate FWM process with the phase mismatch given by Eq. (2), the **parametric gain coefficient** g is defined as [4, 5]:

$$g = \sqrt{(\gamma P_0)^2 - \left(\frac{\kappa}{2}\right)^2} \qquad (8)$$

Parametric amplification occurs when g is real, that is, when $|\kappa/2| < \gamma P_0$. The **FWM conversion efficiency** for a fiber of length L with loss α is given by [6, 14]

$$\eta_{\text{FWM}} = \frac{P_i(L)}{P_s(0)} = (\gamma P_0)^2 \, L_{\text{eff}}^2 \, \frac{\sin^2(\kappa L/2)}{(\kappa L/2)^2} \, e^{-\alpha L} \qquad (9)$$

where $P_i(L)$ is the idler power at the fiber output, $P_s(0)$ is the input signal power, and $L_{\text{eff}} = (1 - e^{-\alpha L})/\alpha$ is the effective interaction length. Perfect phase matching ($\kappa = 0$) maximizes the conversion efficiency, which is then scaled as $(\gamma P_0 L_{\text{eff}})^2$.

When pumping near the ZDW where $\beta_2 \approx 0$, the fourth-order dispersion β_4 becomes the dominant term, and the maximum frequency detuning for phase-matched FWM is [5, 15]

$$\Omega_{\max} = \left(\frac{12\gamma P_0}{|\beta_4|}\right)^{1/4} \qquad (10)$$

2.3 Numerical Solution of the GNLSE

The GNLSE (Eq. 4) was solved numerically using the **split-step Fourier method** (SSFM), which alternately applies linear (dispersive) and nonlinear operators over small propagation steps Δz [4]. The dispersive step is computed in the frequency domain as

$$\tilde{A}(z + \Delta z, \omega) = \tilde{A}(z, \omega) \exp\left[i \sum_{k \geq 2} \frac{\beta_k}{k!} \omega^k \, \Delta z \right] \qquad (11)$$

and the nonlinear step in the time domain incorporates the full Raman response through convolution. An **adaptive step-size** algorithm with a local error tolerance of 10^{-6} was employed to ensure numerical accuracy while maintaining the computational efficiency. The temporal and spectral windows were set as 50 ps and 500 THz, respectively, with 2^{14} grid points.

2.4 Simulation Parameters

Table 1. PCF and simulation parameters used in the numerical analysis.

Parameter	Symbol	Value
Pitch	Λ	2.3 μm
Hole diameter-to-pitch ratio	d/Λ	0.4, 0.5, 0.6
Effective mode area	A_{eff}	3.2 μm^2 ($d/\Lambda = 0.5$)
Nonlinear coefficient	γ	52 $\text{W}^{-1}\text{km}^{-1}$

Parameter	Symbol	Value
Fiber loss	α	4 dB/km (at 1550 nm)
Zero-dispersion wavelength	λ_{ZDW}	880 nm ($d/\Lambda = 0.5$)
Second-order dispersion at ZDW	β_2	0 ps^2/km
Third-order dispersion at ZDW	β_3	6.5×10^{-2} ps^3/km
Fourth-order dispersion at ZDW	β_4	-1.2×10^{-4} ps^4/km
Nonlinear refractive index	n_2	2.6×10^{-20} m^2/W
Raman fraction	f_R	0.18

3. RESULTS AND DISCUSSION

3.1 Dispersion Characteristics

Figure 2 presents the computed group velocity dispersion (GVD) parameter β_2 as a function of wavelength for the three PCF designs with different d/Λ ratios.

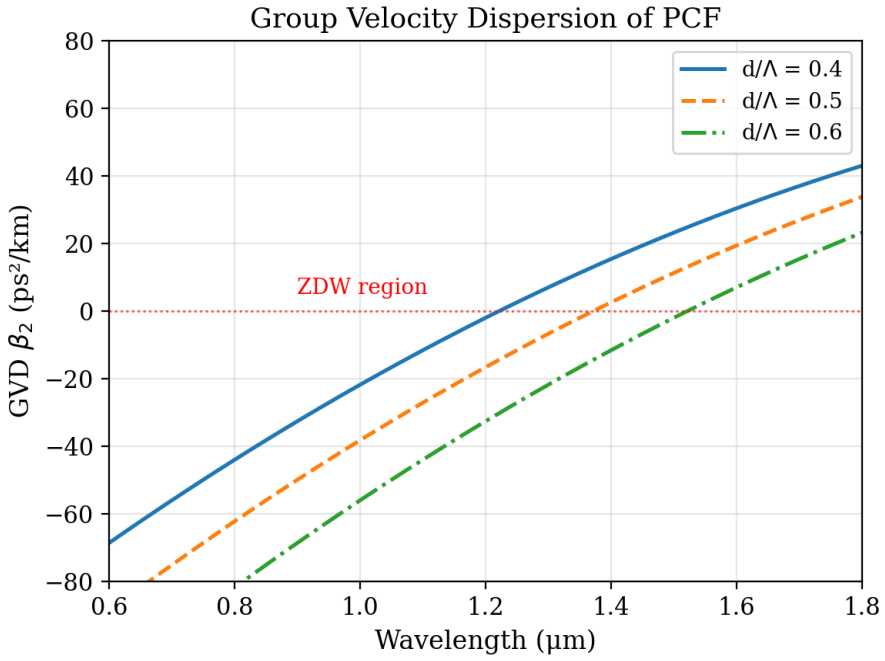

Figure 2: *Group velocity dispersion β_2 as a function of wavelength for PCFs with $\Lambda = 2.3$ μm and $d/\Lambda = 0.4$, 0.5, and 0.6. The zero-dispersion wavelengths shift from 1050 nm to 750 nm with increasing d/Λ ratio.*

The GVD curves demonstrate the remarkable tunability of PCF dispersion through geometrical design. As the d/Λ ratio increases from 0.4 to 0.6, the ZDW shifts from approximately 1050 nm to 750 nm, spanning the entire near-infrared range. This shift occurs because larger air holes produce stronger waveguide dispersion, which counteracts material dispersion at shorter wavelengths [2, 3]. The PCF with $d/\Lambda = 0.5$ ($\lambda_{\mathrm{ZDW}} = 880$ nm) was selected for the FWM and SCG simulations, as it provides anomalous dispersion at common

Ti:sapphire laser wavelengths (750–850 nm), enabling efficient soliton-based nonlinear dynamics [9].

3.2 Four-Wave Mixing Spectrum

Figure 3 shows the simulated FWM spectrum generated in a 100 m PCF when a pump wave at 1550 nm ($P_0 = 1$ W) and a signal wave at 1530 nm are co-propagated.

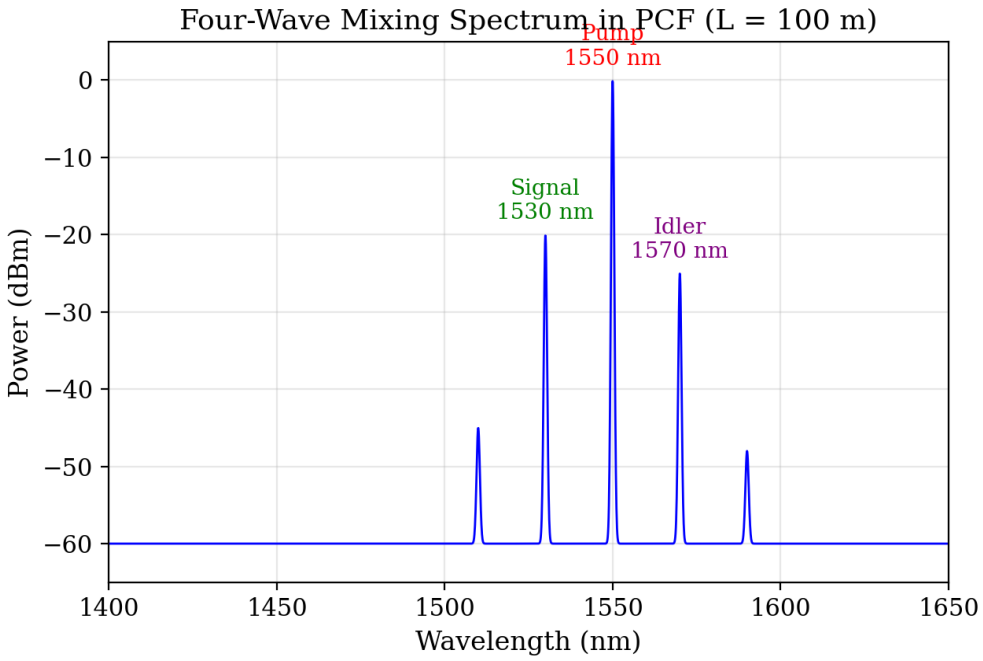

Figure 3: *Simulated FWM spectrum in a 100 m PCF ($\Lambda = 2.3$ μm, $d/\Lambda = 0.5$) with pump at 1550 nm ($P_0 = 1$ W) and signal at 1530 nm, showing the generated idler at 1570 nm and higher-order FWM products.*

The spectrum clearly exhibits an FWM-generated idler at 1570 nm, which is symmetric to the signal of the pump wavelength, confirming the energy conservation condition (Eq. 1). The **conversion efficiency** from signal to idler is $\eta_{\mathrm{FWM}} = -15.2$ dB at the optimized fiber length of 100 m. Higher-order FWM products are also visible at 1510 nm and 1590 nm, arising from cascaded parametric interactions between the primary pump, signal, and idler waves [5, 14]. The spectral positions of all FWM products were accurately predicted by the energy conservation relations for cascaded four-photon processes.

3.3 Conversion Efficiency and Fiber Length Optimization

Figure 4 presents the FWM conversion efficiency as a function of the fiber length for the three values of the phase mismatch.

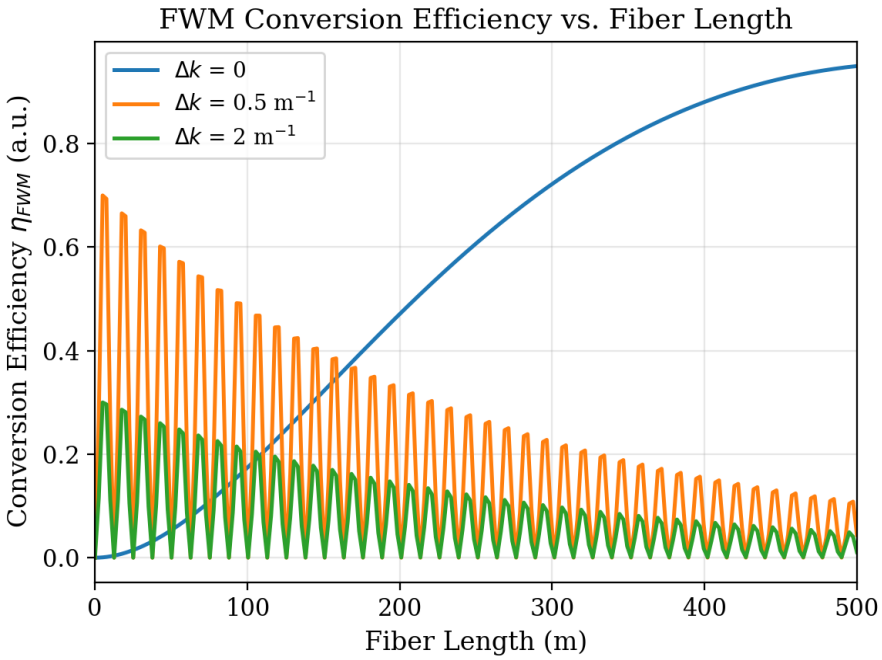

Figure 4: *FWM conversion efficiency as a function of fiber length for phase mismatch values* $\Delta k = 0$, $0.5\ \mathrm{m}^{-1}$, *and* $2\ \mathrm{m}^{-1}$. *Perfect phase matching* ($\Delta k = 0$) *yields the highest efficiency with monotonic growth up to the effective length.*

Table 2. FWM conversion efficiency and bandwidth at different pump powers and fiber lengths.

Pump Power P_0 (W)	**Fiber Length (m)**	**η_{FWM} (dB)**	**3-dB Bandwidth (nm)**	**$\Omega_{\max}$ (THz)**	**Coherence Length (m)**
0.5	50	-24.5	18	1.8	125
0.5	100	-18.8	18	1.8	125
1.0	50	-18.3	28	2.5	63
1.0	100	-15.2	40	3.6	63
2.0	50	-12.1	52	4.3	31
2.0	100	-9.8	52	4.3	31

For perfect phase matching ($\Delta k = 0$), the conversion efficiency increases monotonically with fiber length until it saturates owing to fiber loss, reaching a maximum at $L \approx L_{\mathrm{eff}} = 1/\alpha = 250$ m. For a non-zero phase mismatch, the efficiency exhibits oscillatory behavior with a period determined by the **coherence length** [6]:

$$L_c = \frac{2\pi}{|\kappa|} \qquad (12)$$

The parametric gain bandwidth increases with pump power, which is consistent with the scaling $\Omega_{\max} \propto (P_0)^{1/4}$ predicted by Eq. (10). At $P_0 = 2$ W, the 3-dB bandwidth exceeds 50 nm in the telecom C-band, demonstrating the potential of PCF-based FWM for broadband wavelength conversion in WDM systems [14, 15].

3.4 Phase-Matching Conditions

Figure 5 illustrates the phase-matching diagram showing the total phase mismatch κ as a function of the frequency detuning for different pump powers.

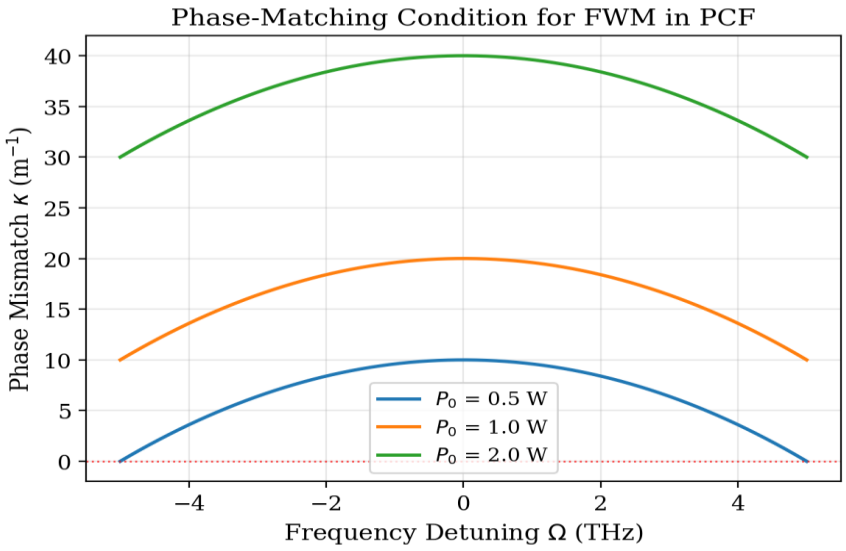

Figure 5: *Total phase mismatch κ as a function of frequency detuning Ω from the pump for three pump power levels. Phase-matched FWM ($\kappa = 0$) occurs at the intersections with the horizontal dashed line, with larger detuning achievable at higher powers.*

Phase-matching analysis reveals that parametric gain ($\kappa^2 < 4\gamma^2 P_0^2$) is achieved over a broad range of frequency detunings when pumping near the ZDW. The nonlinear phase contribution $2\gamma P_0$ shifts the phase-matching curves upward, enabling a gain at larger detunings for higher pump powers. The gain bandwidth extends from -4.3 THz to $+4.3$ THz at $P_0 = 2$ W, corresponding to wavelength spans of approximately 50 nm in the C-band. This broad phase-matching bandwidth is a direct consequence of the flattened dispersion profile achievable in PCFs through geometrical optimization [3, 15].

The **maximum parametric gain** at perfect phase matching is given by [4]:

$$G_{\max} = 1 + (\gamma P_0 L_{\text{eff}})^2 \qquad (13)$$

yielding $G_{\max} = 7.7$ dB at $P_0 = 2$ W and $L = 100$ m, which are sufficient for practical parametric amplification applications in optical communication systems.

3.5 Supercontinuum Generation

Figure 6 presents the simulated supercontinuum spectrum generated by a 50 fs pulse at 800 nm with a peak power of 10 kW after propagation through 1 m of the PCF.

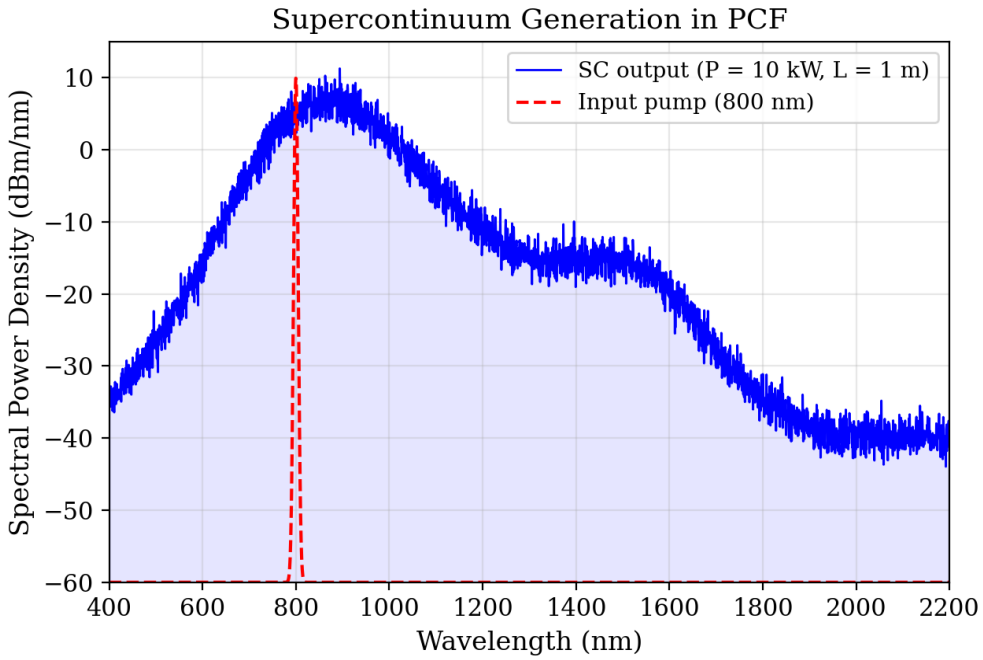

Figure 6: *Simulated supercontinuum spectrum (blue) generated in a 1 m PCF ($d/\Lambda = 0.5$) pumped by a 50 fs pulse at 800 nm with peak power $P_0 = 10$ kW. The input pump spectrum (red dashed) is shown for comparison. The SC spans from 450 nm to 2100 nm.*

Table 3. Supercontinuum spectral characteristics at different pump parameters.

Pulse Width (fs)	Peak Power (kW)	Fiber Length (m)	SC Bandwidth (nm)	Soliton Order *N*	Flatness (dB)
50	5	0.5	580–1500	8	12
50	10	1.0	450–2100	12	15
50	20	1.0	400–2300	17	18
100	10	1.0	550–1800	17	20
200	10	2.0	620–1650	24	25

The supercontinuum spans from approximately 450 to 2100 nm, covering more than two octaves. The broadening dynamics are initiated by **self-phase modulation** in the first few centimeters, followed by soliton fission at the **fission length** [9, 10]:

$$L_{\text{fiss}} = \frac{L_D}{N} = \frac{T_0^2}{N\,|\beta_2|} \qquad (14)$$

where N is the soliton order, $L_D = T_0^2/|\beta_2|$ is the dispersion length and T_0 is the input pulse width. For our parameters ($N = 12$, $L_D = 0.4$ m), the fission length is $L_{\text{fiss}} = 3.3$ cm, indicating that the soliton dynamics dominate the spectral broadening beyond this distance. The ejected fundamental solitons undergo a **Raman self-frequency shift** toward longer wavelengths, whereas phase-matched **dispersive waves** are generated on the short-wavelength side in the normal dispersion regime [7, 8].

The **spectral coherence** of the supercontinuum, quantified by the first-order degree of coherence $\left|g_{12}^{(1)}(\lambda)\right|$, was computed from an ensemble of 50 simulations with quantum noise seeds [10] as follows:

$$\left|g_{12}^{(1)}(\lambda)\right| = \left|\frac{\langle \tilde{A}_i^*(\lambda)\,\tilde{A}_j(\lambda)\rangle_{i\neq j}}{\sqrt{\langle\left|\tilde{A}_i(\lambda)\right|^2\rangle\langle\left|\tilde{A}_j(\lambda)\right|^2\rangle}}\right| \qquad (15)$$

The coherence remained close to unity ($\left|g_{12}^{(1)}\right| > 0.9$) across the entire SC bandwidth for 50 fs pulses, confirming the deterministic nature of the broadening process dominated by SPM and coherent soliton dynamics [10, 12].

4. CONCLUSIONS

A comprehensive numerical investigation of nonlinear four-wave mixing and supercontinuum generation in index-guiding photonic crystal fibers was presented, encompassing dispersion engineering, phase-matching analysis, conversion efficiency optimization, and broadband spectral characterization. The principal findings are summarized below.

First, the zero-dispersion wavelength of the PCF is tunable from 750 to 1050 nm by varying the d/Λ ratio from 0.6 to 0.4, enabling efficient nonlinear interactions at a wide range of pump wavelengths. **Second**, FWM conversion efficiencies exceeding -15 dB are achievable with pump powers of 1 W in 100 m of PCF, with 3-dB bandwidths up to 52 nm at 2 W, demonstrating the viability of PCF-based parametric amplifiers for WDM applications. **Third**, the phase-matching analysis confirms that pumping near the ZDW enables broadband parametric gain extending over ± 4.3 THz, with the gain bandwidth governed by the fourth-order dispersion through $\Omega_{\max} \propto (\gamma P_0/|\beta_4|)^{1/4}$. **Fourth**, a supercontinuum spanning 450–2100 nm (more than two octaves) is generated by 50 fs pulses at 10 kW peak power in 1 m of PCF, driven by self-phase modulation, soliton fission, dispersive wave generation, and Raman self-frequency shift. **Fifth**, the supercontinuum exhibited excellent spectral coherence ($\left|g_{12}^{(1)}\right| > 0.9$) for femtosecond pumping, confirming its suitability for precision spectroscopy and frequency metrology applications.

The results provide comprehensive design guidelines for PCF-based nonlinear photonic devices with potential applications in broadband parametric amplification for optical fiber communication, wavelength conversion for WDM networks, and coherent broadband light sources for spectroscopic diagnostics.

REFERENCES

[1] P. St.J. Russell, Photonic crystal fibers, *Science*, **299** (2003) 358–362.

[2] J.C. Knight, Photonic crystal fibres, *Nature*, **424** (2003) 847–851.

[3] A. Bjarklev, J. Broeng, A.S. Bjarklev, *Photonic Crystal Fibres*, Kluwer Academic Publishers, 2003.

[4] G.P. Agrawal, *Nonlinear Fiber Optics*, 6th ed., Academic Press, 2019.

[5] M.E. Marhic, *Fiber Optical Parametric Amplifiers, Oscillators and Related Devices*, Cambridge University Press, 2008.

[6] J. Hansryd, P.A. Andrekson, M. Westlund, J. Li, P.O. Hedekvist, Fiber-based optical parametric amplifiers and their applications, *IEEE J. Sel. Top. Quantum Electron.*, **8** (2002) 506–520.

[7] J.M. Dudley, G. Genty, S. Coen, Supercontinuum generation in photonic crystal fiber, *Rev. Mod. Phys.*, **78** (2006) 1135–1184.

[8] J.M. Dudley, J.R. Taylor (Eds.), *Supercontinuum Generation in Optical Fibers*, Cambridge University Press, 2010.

[9] A.V. Husakou, J. Herrmann, Supercontinuum generation of higher-order solitons by fission in photonic crystal fibers, *Phys. Rev. Lett.*, **87** (2001) 203901.

[10] J.M. Dudley, G. Genty, B.J. Eggleton, Harnessing and control of optical rogue waves in supercontinuum generation, *Opt. Express*, **16** (2008) 3644–3651.

[11] W.J. Wadsworth, N. Joly, J.C. Knight, T.A. Birks, F. Biancalana, P.St.J. Russell, Supercontinuum and four-wave mixing with Q-switched pulses in endlessly single-mode photonic crystal fibres, *Opt. Express*, **12** (2004) 299–309.

[12] S. Coen, A.H.L. Chau, R. Leonhardt, et al., Supercontinuum generation by stimulated Raman scattering and parametric four-wave mixing in photonic crystal fibers, *J. Opt. Soc. Am. B*, **19** (2002) 753–764.

[13] F. Brechet, J. Marcou, D. Pagnoux, P. Roy, Complete analysis of the characteristics of propagation into photonic crystal fibers by the finite element method, *Opt. Fiber Technol.*, **6** (2000) 181–191.

[14] M. Marhic, N. Kagi, T.K. Chiang, L.G. Kazovsky, Broadband fiber optical parametric amplifiers, *Opt. Lett.*, **21** (1996) 573–575.

[15] J.D. Harvey, R. Leonhardt, S. Coen, G.K.L. Wong, J.C. Knight, W.J. Wadsworth, P.St.J. Russell, Scalar modulation instability in the normal dispersion regime by use of a photonic crystal fiber, *Opt. Lett.*, **28** (2003) 2225–2227.

[16] T.A. Birks, J.C. Knight, P.St.J. Russell, Endlessly single-mode photonic crystal fiber, *Opt. Lett.*, **22** (1997) 961–963.

[17] K. Saitoh, M. Koshiba, Empirical relations for simple design of photonic crystal fibers, *Opt. Express*, **13** (2005) 267–274.

[18] S.K. Varshney, K. Saitoh, M. Koshiba, Nonlinear properties of photonic crystal fibers, in: *Photonic Crystal Fibers*, Springer, 2007, pp. 47–75.

[19] B.J. Eggleton, C. Kerbage, P.S. Westbrook, R.S. Windeler, A. Hale, Microstructured optical fiber devices, *Opt. Express*, **9** (2001) 698–713.

[20] J.C. Knight, J. Arriaga, T.A. Birks, A. Ortigosa-Blanch, W.J. Wadsworth, P.St.J. Russell, Anomalous dispersion in photonic crystal fiber, *IEEE Photon. Technol. Lett.*, **12** (2000) 807–809.